

Adaptive Inference through Bayesian and Inverse Bayesian Inference with Symmetry-Bias in  
Nonstationary Environments

Shuji Shinohara<sup>a,\*</sup>, Daiki Morita<sup>a</sup>, Hayato Hirai<sup>a</sup>, Ryosuke Kuribayashi<sup>a</sup>, Nobuhito Manome<sup>b,c</sup>, Toru  
Moriyama<sup>d</sup>, Yoshihiro Nakajima<sup>e</sup>, Yukio-Pegio Gunji<sup>f</sup>, and Ung-il Chung<sup>b</sup>

<sup>a</sup> School of Science and Engineering, Tokyo Denki University, Saitama, Japan

<sup>b</sup> Department of Bioengineering, Graduate School of Engineering, The University of Tokyo, Tokyo, Japan

<sup>c</sup> Department of Research and Development, SoftBank Robotics Group Corp., Tokyo, Japan

<sup>d</sup> Faculty of Textile Science, Shinshu University, Ueda, Japan

<sup>e</sup> Graduate School of Economics, Osaka City University, Osaka, Japan

<sup>f</sup> Department of Intermedia Art and Science, School of Fundamental Science and Technology, Waseda  
University, Tokyo, Japan

\* Corresponding author

E-mail: s.shinohara@mail.dendai.ac.jp

Postal address: School of Science and Engineering, Tokyo Denki University, Ishizaka, Hatoyama-machi,  
Hiki-gun, Saitama 350-0394, Japan

## Abstract

This study introduces a novel inference framework, designated as Bayesian and inverse Bayesian (BIB) inference, which concurrently performs both conventional and inverse Bayesian updates by integrating symmetry bias into Bayesian inference. The effectiveness of the model was evaluated through a sequential estimation task involving observations sampled from a Gaussian distribution with a stochastically time-varying mean.

Conventional Bayesian inference entails a fundamental trade-off between adaptability to abrupt environmental shifts and estimation accuracy during stable intervals. The BIB framework addresses this limitation by dynamically modulating the learning rate through inverse Bayesian updates, thereby enhancing adaptive flexibility. The BIB model generated spontaneous bursts in the learning rate during sudden environmental transitions, transiently entering a high-sensitivity state to accommodate incoming data. This intermittent burst-relaxation pattern functions as a dynamic mechanism that balances adaptability and accuracy.

Further analysis of burst interval distributions demonstrated that the BIB model consistently produced power-law distributions under diverse conditions. Such robust scaling behavior, absent in conventional Bayesian inference, appears to emerge from a self-regulatory mechanism driven by inverse Bayesian updates. These results present a novel computational perspective on scale-free phenomena in natural systems and offer implications for designing adaptive inference systems in nonstationary environments.

**Keywords:** Bayesian inference, Inverse Bayesian inference, Symmetry bias, Learning rate dynamics, Power-law distribution, Self-organized criticality

## 1 Introduction

Prediction and action selection based on external information are fundamental to human cognitive processes. In recent years, such predictive behavior has increasingly been interpreted through the frameworks of the free energy principle, active inference, and predictive error minimization [1–3]. The free-energy principle is formally grounded in Bayesian inference [1, 4], and the role of Bayesian inference in brain function has garnered growing interest in neuroscience research [5, 6].

Bayesian inference provides a normative framework for estimating latent causes from observed data and has been widely applied across cognitive science, artificial intelligence, and statistics. This framework entails updating posterior probabilities based on prior beliefs and observations, followed by the recursive use of the posterior as the subsequent prior to identify the most plausible hypothesis. However, human reasoning frequently diverges from normative Bayesian rationality and exhibits systematic cognitive biases. For example, when confronted with a unidirectional conditional statement such as “if  $p$ , then  $q$ ,” individuals often infer the converse “if  $q$ , then  $p$ ” or the contraposition “if not  $p$ , then not  $q$ .” These tendencies are referred to as the symmetry bias and the mutual exclusivity bias, respectively [7–10]. Such reasoning patterns deviate from classical logic and reflect fundamental features of intuitive human inference.

In the field of causal induction, substantial research has examined how individuals assess the strength of causal relationships based on the co-occurrence of events. Confidence in a conditional statement such as “if  $p$ , then  $q$ ” is generally considered proportional to the conditional probability of  $q$  given  $p$  [11]. However, a strong perceived causal link between cause  $c$  and effect  $e$  requires not only a high predictive probability ( $P(e|c)$ ), but also a high diagnostic probability ( $P(c|e)$ ). The geometric mean of these two conditional probabilities can serve as an effective approximation of causal strength [12]. These findings underscore the importance of symmetry in causal reasoning.

The accumulation of observational data improves the accuracy of causal estimation; however, this holds only when the data are generated by a consistent underlying cause. In nonstationary environments, where causal factors evolve over time, inference must rely primarily on recent data to maintain responsiveness. This necessity induces a trade-off between estimation accuracy and adaptability to change. Shinohara et al. [13] proposed a model that incorporates symmetry bias into Bayesian inference and demonstrated its effectiveness in nonstationary environments by including mechanisms such as forgetting older data and dynamically updating likelihoods.

Bayesian updating is formally defined as  $P_{t+1}(h) \leftarrow P_t(h | d_t)$ , where  $h$  denotes a hypothesis and  $d_t$  represents the observed data at time  $t$ . Gunji et al. [14] introduced inverse Bayesian updating, formulated as  $P_{t+1}(d_t | h) \leftarrow P_t(d_t)$ , by reversing the direction of inference between  $h$  and  $d$ . They demonstrated that the combination of Bayesian and inverse Bayesian updates can effectively model behaviors such as animal swarming and human decision-making [15–17].

Previous studies have typically assumed a discrete hypothesis space, which limits applicability to problems involving continuous estimation. Hence, this study provides a theoretical formulation of a Bayesian inference model incorporating symmetry bias under the assumption of a Gaussian prior distribution.

The proposed model aligns with the definition of inverse Bayesian updating by Gunji et al. [14], particularly in its incorporation of a likelihood variance expansion process.

The expansion operation functions by blurring distinctions between hypotheses. Specifically,

- Bayesian updating sharpens the hypothesis space, reducing uncertainty,
- whereas inverse Bayesian updating broadens it, diminishing differences among hypotheses.

These bidirectional beliefs updating mechanisms operate simultaneously.

The proposed model was used to estimate the mean of a Gaussian distribution from sequentially observed data, where the mean changed stochastically over time. Conventional Bayesian inference applied

to this task exhibited a trade-off between estimation accuracy and adaptability. However, the proposed model, which incorporated inverse Bayesian updating, effectively overcame this trade-off. Moreover, the proposed model universally exhibited scale-free behavior in its inference dynamics. The implications of this finding are further discussed in relation to self-organized criticality (SOC).

## 2 Material and methods

### 2.1 Bayesian and inverse Bayesian inference (BIB) with symmetry bias

We introduce a symmetry bias as follows based on the study by Shinohara et al. [12].

$$P_{t+1}(h|d) \leftarrow P_t(h|d)^{1-\beta} P_t(d|h)^\beta \quad (1)$$

$$P_{t+1}(d|h) \leftarrow P_t(d|h)^{1-\beta} P_t(h|d)^\beta \quad (2)$$

The parameter  $0 \leq \beta \leq 1$  represents the strength of the symmetry bias. When  $\beta = 0$ , Eqs. (1) and (2) become each identity and nothing changes. When  $\beta = 0.5$ , Eqs. (1) and (2) become  $P_{t+1}(h|d) = P_{t+1}(d|h) = \sqrt{P_t(d|h)P_t(h|d)}$ , and symmetry holds. Eqs. (1) and (2) can be transformed as follows using Bayes' theorem.

$$P_{t+1}(h|d) \leftarrow \left( \frac{P_t(h)}{P_t(d)} \right)^{1-\beta} P_t(d|h) \quad (3)$$

$$P_{t+1}(d|h) \leftarrow \left( \frac{P_t(h)}{P_t(d)} \right)^\beta P_t(d|h) \quad (4)$$

Using Bayesian update, we rewrite Eq. (3) as follows:

$$P_{t+1}(h) \leftarrow \left( \frac{P_t(h)}{P_t(d_t)} \right)^{1-\beta} P_t(d_t|h). \quad (5)$$

When  $\beta = 0$ , the formulation reduces to standard Bayesian inference, and Eq. (4) becomes

$P_{t+1}(d_t | h) \leftarrow P_t(d_t | h)$ ; the likelihood distribution does not change.

In Eq. (5),  $P_t(d_t)$  is common across all the hypotheses and therefore can be considered a constant.

Moreover,  $P_{t+1}(h) \propto P_0(h)^{(1-\beta)^t} \dots P_{t-i}(d_{t-i} | h)^{(1-\beta)^i} \dots P_{t-2}(d_{t-2} | h)^{(1-\beta)^2} P_{t-1}(d_{t-1} | h)^{(1-\beta)} P_t(d_t | h)$  holds due to the recursiveness of  $P(h)$  [13].

This formulation implies that likelihoods corresponding to older observations are progressively discounted when  $\beta > 0$ , exerting decreasing influence on the current prior distribution. Hence,  $\beta$  can be interpreted as a discount factor or forgetting rate.

Consider Bayesian inference applied to estimating the mean of a Gaussian distribution that generates the observed data. Let the hypothesis  $h$  represent the mean  $\mu$  of the Gaussian distribution. Define the prior distribution of  $\mu$  as:

$$P_t(\mu) = \frac{1}{\sqrt{2\pi\Phi_t}} \exp\left[-\frac{1}{2\Phi_t}(\mu - \theta_t)^2\right] \quad (6)$$

where  $\Phi_t$  and  $\theta_t$  denote the variance and mean of the prior distribution, respectively. The term  $\mu = \theta_t$  corresponds to the most confident hypothesis at time  $t$ , i.e., the current estimate. The likelihood is also modeled as a Gaussian distribution:

$$P_t(d | \mu) = \frac{1}{\sqrt{2\pi\Sigma_t}} \exp\left[-\frac{1}{2\Sigma_t}(d - \mu)^2\right] \quad (7)$$

where  $\Sigma_t$  denotes the likelihood variance.

Substituting  $P_t(h)$  and  $P_t(d_t | h)$  in Eq. (5) with the  $P_t(\mu)$  and  $P_t(d_t | \mu)$  in Eqs. (6) and (7), respectively, yields:

$$\begin{aligned}
P_{t+1}(\mu) &\propto [P_t(\mu)]^{1-\beta} P_t(d_t | \mu) \\
&\propto \left[ \exp \left[ -\frac{1}{2\Phi_t} (\mu - \theta_t)^2 \right] \right]^{1-\beta} \exp \left[ -\frac{1}{2\Sigma_t} (d_t - \mu)^2 \right] \\
&= \exp \left[ -\frac{1}{2} \left[ \frac{(1-\beta)(\mu - \theta_t)^2}{\Phi_t} + \frac{(d_t - \mu)^2}{\Sigma_t} \right] \right]
\end{aligned} \tag{8}$$

The prior distribution can be updated by rearranging Eq. (8) as follows:

$$\begin{aligned}
P_{t+1}(\mu) &= \frac{1}{\sqrt{2\pi\Phi_{t+1}}} \exp \left[ -\frac{1}{2\Phi_{t+1}} [\mu - \theta_{t+1}]^2 \right] \\
\Phi_{t+1} &= \left( \frac{(1-\beta)}{\Phi_t} + \frac{1}{\Sigma_t} \right)^{-1} = \frac{\Phi_t}{\Phi_t + (1-\beta)\Sigma_t} \Sigma_t \\
\theta_{t+1} &= \frac{(1-\beta)\Sigma_t}{\Phi_t + (1-\beta)\Sigma_t} \theta_t + \frac{\Phi_t}{\Phi_t + (1-\beta)\Sigma_t} d_t
\end{aligned} \tag{9}$$

Let  $\alpha_{t+1} = \frac{\Phi_t}{\Phi_t + (1-\beta)\Sigma_t}$  denote the learning rate.  $\Phi_{t+1}$  and  $\theta_{t+1}$  can be rewritten as follows using the learning rate.

$$\Phi_{t+1} = \alpha_{t+1} \Sigma_t \tag{10}$$

$$\theta_{t+1} = (1 - \alpha_{t+1}) \theta_t + \alpha_{t+1} d_t \tag{11}$$

These results confirm that Eq. (5) describes Bayesian updating with a discount factor. However, the interpretation of Eq. (4) remains to be addressed. Substituting  $P_t(\mu)$  and  $P_t(d_t | \mu)$  with  $P_t(h)$  and  $P_t(d_t | h)$ , Eq. (4) becomes:

$$\begin{aligned}
P_{t+1}(d | \mu) &\leftarrow \left[ \frac{P_t(\mu)}{P_t(d)} \right]^\beta P_t(d | \mu) \\
&\propto \left[ \exp \left[ -\frac{1}{2\Phi_t} (\mu - \theta_t)^2 \right] \right]^\beta \exp \left[ -\frac{1}{2(\Sigma_t + \Phi_t)} (d - \theta_t)^2 \right]^{-\beta} \exp \left[ -\frac{1}{2\Sigma_t} (d - \mu)^2 \right] \\
&= \exp \left[ -\frac{1}{2} \left[ \frac{\beta}{\Phi_t} (\mu - \theta_t)^2 - \frac{\beta}{\Sigma_t + \Phi_t} (d - \theta_t)^2 + \frac{(d - \mu)^2}{\Sigma_t} \right] \right] \\
&= \exp \left[ -\frac{1}{2} \left[ \left( \frac{1}{\Sigma_t} - \frac{\beta}{\Sigma_t + \Phi_t} \right) d^2 - 2 \left( \frac{\mu}{\Sigma_t} - \frac{\beta\theta_t}{\Sigma_t + \Phi_t} \right) d - \frac{\beta\theta_t^2}{\Sigma_t + \Phi_t} + \frac{\mu^2}{\Sigma_t} + \frac{\beta}{\Phi_t} (\mu - \theta_t)^2 \right] \right] \\
&\propto \exp \left[ -\frac{1}{2} \left[ \left( \frac{1}{\Sigma_t} - \frac{\beta}{\Sigma_t + \Phi_t} \right) d^2 - 2 \left( \frac{\mu}{\Sigma_t} - \frac{\beta\theta_t}{\Sigma_t + \Phi_t} \right) d \right] \right] \\
&\propto \exp \left[ -\frac{1}{2} \left( \frac{1}{\Sigma_t} - \frac{\beta}{\Sigma_t + \Phi_t} \right) \left[ d - \left( \frac{1}{\Sigma_t} - \frac{\beta}{\Sigma_t + \Phi_t} \right)^{-1} \left( \frac{\mu}{\Sigma_t} - \frac{\beta\theta_t}{\Sigma_t + \Phi_t} \right) \right]^2 \right]
\end{aligned} \tag{12}$$

where  $P_t(d) = \int P_t(\mu) P_t(d | \mu) d\mu = \frac{1}{\sqrt{2\pi(\Sigma_t + \Phi_t)}} \exp \left[ -\frac{1}{2(\Sigma_t + \Phi_t)} (d - \theta_t)^2 \right]$  was used.

The likelihood can be written as follows by rearranging Eq. (12):

$$\begin{aligned}
P_{t+1}(d | \mu') &= \frac{1}{\sqrt{2\pi\Sigma_{t+1}}} \exp \left[ -\frac{1}{2\Sigma_{t+1}} (d - \mu')^2 \right] \\
\mu' &= \Sigma_{t+1} \left( \frac{\mu}{\Sigma_t} - \frac{\beta\theta_t}{\Sigma_t + \Phi_t} \right) \\
\Sigma_{t+1} &= \left( \frac{1}{\Sigma_t} - \frac{\beta}{\Sigma_t + \Phi_t} \right)^{-1} = \frac{\Phi_t + \Sigma_t}{\Phi_t + (1 - \beta)\Sigma_t} \Sigma_t
\end{aligned} \tag{13}$$

Given that  $\mu$  is a continuous variable, replacing  $\mu'$  with  $\mu$  in Eq. (13) yields:

$$\begin{aligned}
P_{t+1}(d | \mu) &= \frac{1}{\sqrt{2\pi\Sigma_{t+1}}} \exp \left[ -\frac{1}{2\Sigma_{t+1}} (d - \mu)^2 \right] \\
\Sigma_{t+1} &= \frac{\Phi_t + \Sigma_t}{\Phi_t + (1 - \beta)\Sigma_t} \Sigma_t
\end{aligned} \tag{14}$$



If  $\beta > 0$ , then  $\frac{\Phi_t + \Sigma_t}{\Phi_t + (1 - \beta)\Sigma_t} > 1$ , resulting in an increasing likelihood variance  $\Sigma$ . Hence, Eq. (14)

represents a variance-expanding update. Hereafter, this likelihood update process is referred to as an inverse Bayesian update.

Gunji et al. [14] defined inverse Bayesian updating as  $P(d|\mu) \leftarrow P(d)$ . As noted earlier,

$$P_t(d) = \int P_t(\mu)P_t(d|\mu)d\mu = \frac{1}{\sqrt{2\pi(\Sigma_t + \Phi_t)}} \exp\left[-\frac{1}{2(\Sigma_t + \Phi_t)}(d - \theta_t)^2\right] \text{ holds, where } P_t(d) \text{ represents}$$

the weighted average of the individual likelihoods  $P_t(d|\mu)$ . Inverse Bayesian updating involves substituting individual likelihoods with the global average.

The variance of  $P_t(d|\mu)$  is  $\Sigma_t$ , whereas that of  $P_t(d)$  is  $\Sigma_t + \Phi_t$ . Therefore, inverse Bayesian updating can be interpreted as a process that expands the likelihood variance from  $\Sigma_t$  to  $\Sigma_t + \Phi_t$ .

Compared to Eq. (14), both processes increase the variance of the likelihood. Gunji's definition of inverse

Bayes updating corresponds to the case where  $\beta = \frac{\Phi_t}{\Sigma_t}$  is used in Eq. (14). Hereafter, the method involving

only Bayesian updating with a discount rate, governed by Eqs. (10) and (11), is referred to as Bayesian inference. However, the proposed model, which combines Bayesian and inverse Bayesian updates by incorporating Eq. (14), is referred to as Bayesian and inverse Bayesian (BIB) inference.

Under Bayesian inference, Eq. (14) is not used to update the likelihood; hence, the likelihood remains fixed at  $\Sigma_t = \Sigma_0$ . In this case,  $\Phi_{t+1} = \alpha_{t+1}\Sigma_0 \propto \alpha_{t+1}$  holds from Eq. (10), and the variances of the prior distribution are proportional to the learning rate. Specifically, the prior variance is given by

$$\Phi_{t+1} = \alpha_{t+1}\Sigma_0 = \frac{\Phi_t}{\Phi_t + (1 - \beta)\Sigma_0}\Sigma_0, \text{ and the learning rate is } \alpha_{t+1} = \frac{\Phi_t}{\Phi_t + (1 - \beta)\Sigma_0}, \text{ implying } \lim_{t \rightarrow \infty} \Phi_t = \beta\Sigma_0,$$

and thus  $\lim_{t \rightarrow \infty} \alpha_t = \beta$ . Specifically, the learning and discount rates reach equilibrium over time.

When the discount rate  $\beta$  is 0, both the prior variance and the learning rate asymptotically converge to 0. This behavior reflects increasing confidence in the estimate  $\theta_t$  as more data are accumulated, ultimately leading to the exclusion of new information from subsequent observations. However, when a nonzero discount rate is applied ( $\beta > 0$ ), the variance of the prior distribution and learning rate do not become zero because the influence of past observations is limited by the forgetting mechanism. Consequently, new data continue to inform the estimate at a constant rate determined by the discount factor  $\beta$ .

The likelihood variance  $\Sigma_t$  increases with each update in BIB inference. With respect to the prior variance,  $\Phi_{t+1} = \alpha_{t+1}\Sigma_t = \frac{\Phi_t}{\Phi_t + (1-\beta)\Sigma_t}\Sigma_t = \frac{1}{\Phi_t/\Sigma_t - \beta + 1}\Phi_t$  holds. Hence, after the point at which  $\Sigma_t$  increases and  $\frac{\Phi_t}{\Sigma_t} < \beta$  holds,  $\Phi_t$  also increases and diverges over time. Consequently, the prior distribution becomes uniform over all values of  $\mu$ , effectively eliminating distinctions among hypotheses. Hence, BIB inference performs two mutually opposing operations: Bayesian updating progressively narrows the set of plausible hypotheses based on observed data, whereas inverse Bayesian updating disrupts the foundational premise of Bayesian inference—namely, the identification of a single, most plausible hypothesis.

Here, we introduced a set of discrete reference points  $\mu^0, \mu^1, \dots, \mu^i, \dots, \mu^N$  to detect changes in the data-generating distribution. We defined the hypothesis with the highest confidence at time  $t$  as  $\mu_t^{\max} = \arg \max \left( P_t(\mu^i) \right)$ . We considered the generating distribution to change in the case of  $\mu_{t+1}^{\max} \neq \mu_t^{\max}$  and reset the variance to  $\Sigma_t = \Sigma_0$ .

In both cases, the hypothesis with the highest posterior confidence may change. The first occurs when the observed data significantly deviates from the previously estimated values. According to Eq. (11), a large discrepancy between the estimate  $\theta_t$  and the observed data  $d_t$ , combined with a high learning rate  $\alpha_{t+1}$ , results in a substantial update to  $\theta_t$ . In such cases, the prior distribution of the  $P_{t+1}(\mu)$  changes substantially,

potentially altering the most confident hypothesis. This change can be interpreted as anomaly detection in the incoming data.

The second case is when the variances of the likelihood and the prior diverge because of inverse Bayes update.

In this case, the confidence levels across hypotheses become indistinguishable owing to

$P(\mu^0) = P(\mu^1) = \dots = P(\mu^i) = \dots = P(\mu^N) = 0$ , and the most confident hypothesis is selected randomly.

Strictly speaking, when the likelihood variance diverges, the likelihood function no longer satisfies the definition of a proper probability distribution. This condition does not imply that all hypotheses become equally plausible, but rather that all hypotheses effectively vanish. The inability to determine a single hypothesis with maximal confidence does not stem from multiple hypotheses having the same confidence level, but from the fact that the very problem of selecting an optimal hypothesis becomes ill-defined.

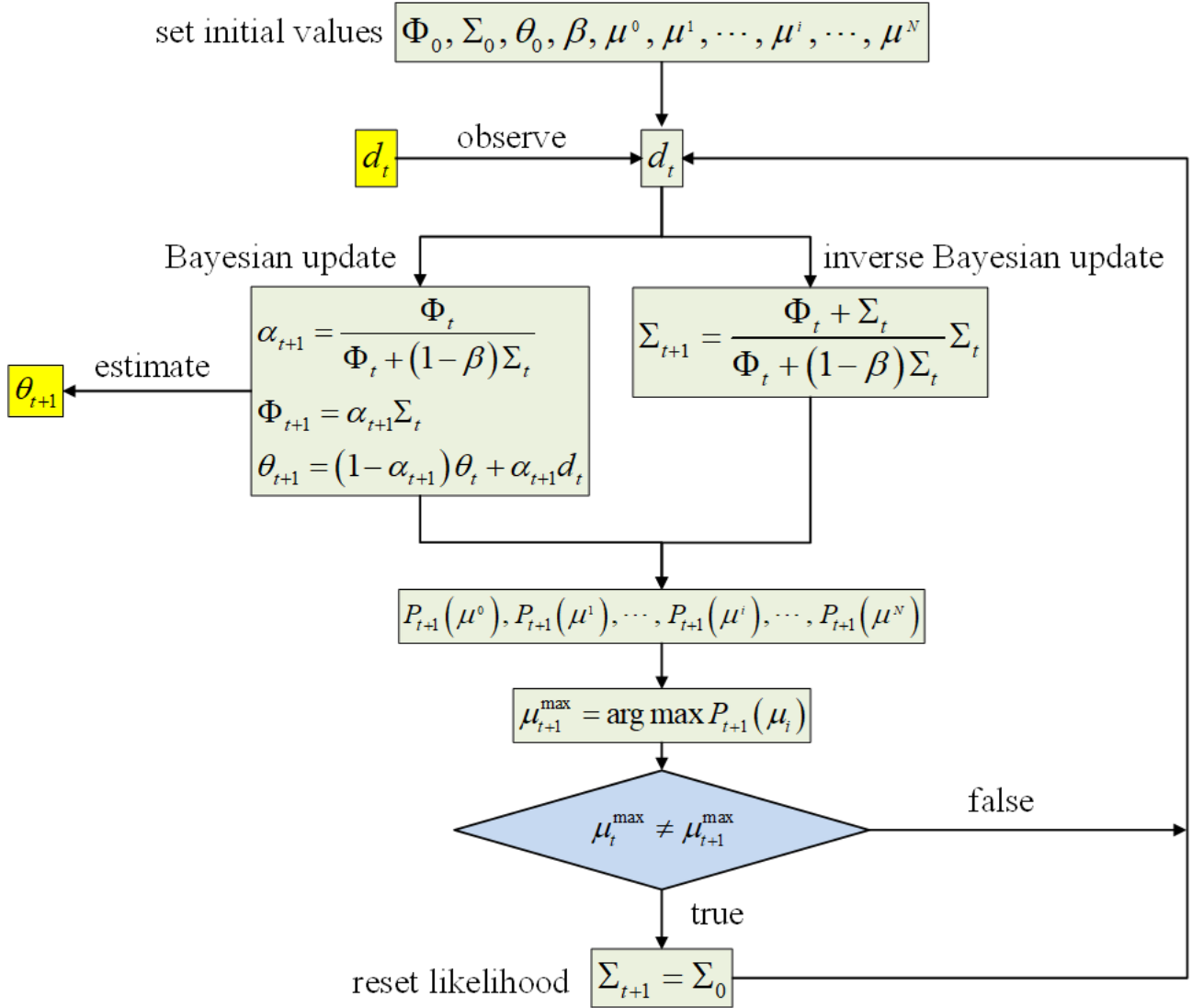


**Fig. 1** Computational procedures for Bayesian inference and BIB inference. Inverse Bayesian update was not performed in Bayesian inference

Fig. 1 illustrates the procedures for Bayesian and BIB inferences. In Bayesian inference without inverse Bayesian updating, resets occur frequently due to the first scenario. However, the inference process remains unaffected by resets because the likelihood variance remains fixed. However, a burst in the learning rate occurs in the BIB inference, when the variance  $\Sigma_t$  of the expanded likelihood is reset to  $\Sigma_0$ .

## 2.2 Simulation setting

This study simulated the task of estimating the mean of a normal distribution, generating observed data in a nonstationary environment.

The data-generating distribution was assumed to follow the normal distribution defined as:

$$P_t(d) = \frac{1}{\sqrt{2\pi\Omega}} \exp\left[-\frac{1}{2\Omega}(d - \eta_t)^2\right] \quad (15)$$

The variance was fixed at  $\Omega = 0.09$ . However, the mean  $\eta_t$  varied irregularly. Specifically, a random number  $rnd$  was sampled from the uniform distribution  $U(0, 1)$  at each time step. If  $rnd < 0.001$ , the mean was changed. In such cases, a random number  $rnd\eta$  was sampled from the uniform distribution  $U(-2.5, 2.5)$ , which was then adopted as the new mean.

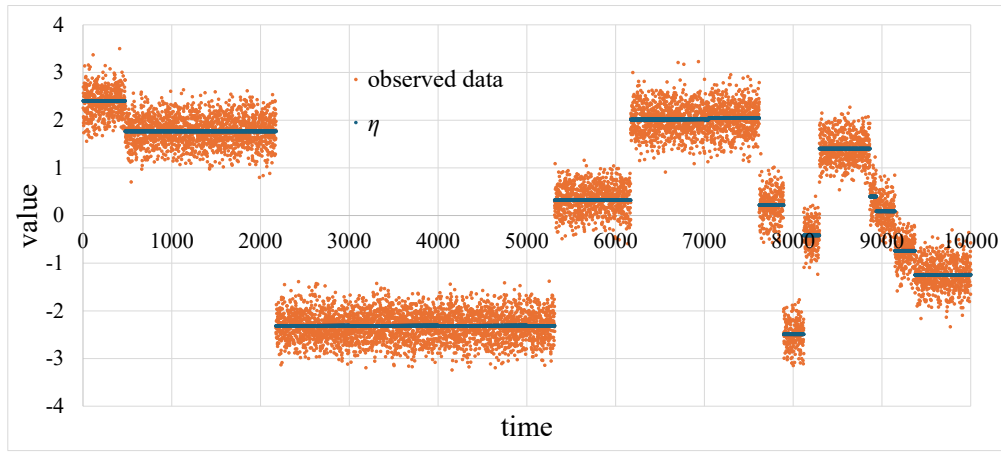
$$\eta_{t+1} = \begin{cases} rnd\eta \sim U(-2.5, 2.5) & \text{if } rnd < 0.001, \text{ } rnd \sim U(0, 1) \\ \eta_t & \text{otherwise} \end{cases} \quad (16)$$

For the discrete hypothesis reference points  $\mu^0, \mu^1, \dots, \mu^i, \dots, \mu^N$ ,  $N = 50$  and the interval between the points was  $\Delta\mu = 0.1$ , fixed at  $\mu^i = -2.5 + i\Delta\mu$ .

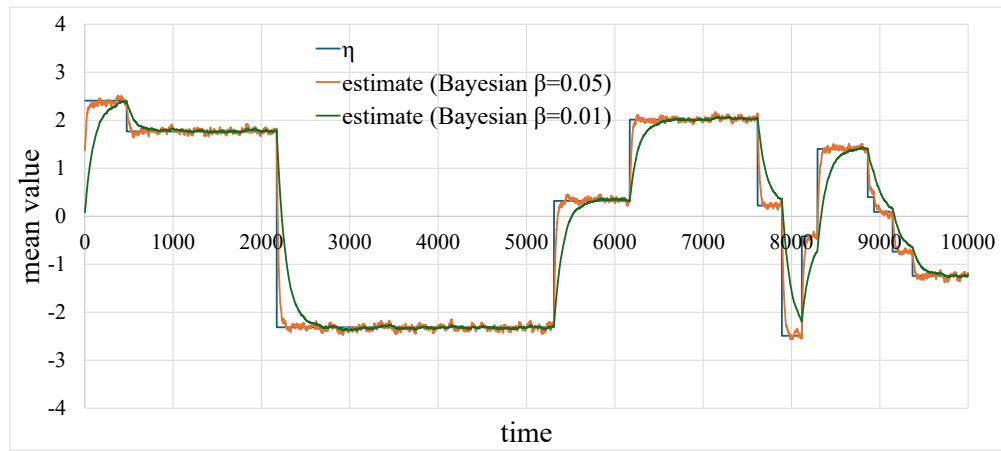
Data from the initial 10,000 time steps were excluded from the analysis to eliminate the influence of transient behavior. Only data from time step 10,001 onward were used.

The simulation was implemented in C++ using MinGW11.2.0 64-bit compiler [18]. The Qt library (Qt version Qt 6.4.0 MinGW 64-bit) was also used for the development [19]. The maximum representable real number in this simulation environment was  $1.79769\text{e}+308$ . Values exceeding this limit were considered as infinity, and their reciprocals were recognized as 0.

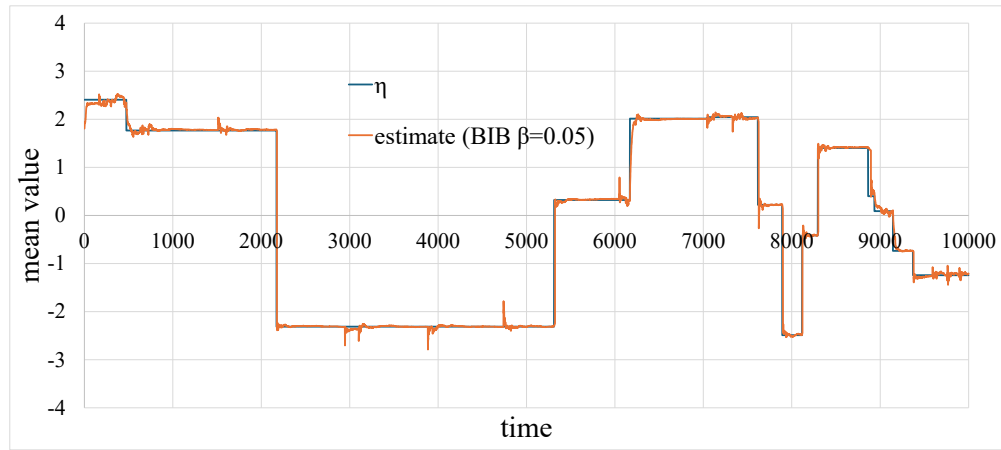
### 3 Results



(a)



(b)



(c)

**Fig. 2** Representative time series of observed data and corresponding estimates. The mean value  $\eta$  of the data generating distribution is indicated. (a) Observed data. (b) Estimates obtained via Bayesian inference ( $\beta = 0.05$ ,  $\beta = 0.01$ ). (c) Estimates obtained by BIB inference ( $\beta = 0.05$ )

Fig. 2(a) presents a representative time series of observed data generated from a normal distribution.

Figs. 2(b) and 2(c) depict examples of the estimated mean values of the data-generating distribution obtained using Bayesian inference and BIB inference, respectively. Each figure includes the true mean value of the generating distribution for reference. The Bayesian estimation (Fig. 2(b)) demonstrates that increasing the discount rate  $\beta$  enhances responsiveness to abrupt changes but reduces accuracy during periods of stability. However, BIB estimation exhibits occasional bursts in the estimated values while achieving both high tracking performance and accuracy.

The interval  $[t', t' + n]$  from a specific time  $t'$ , when the mean of the data-generating distribution changes, to the time immediately preceding the next change, was divided into two equal halves to quantify adaptability to change and estimation accuracy. The root mean square error (RMSE) between the estimated and true values was calculated separately for each half. Specifically, RMSEs were denoted as

$$RMSE_f = \sqrt{\frac{2}{n} \sum_{i=t'}^{t'+n/2-1} (\theta_i - \eta_i)^2} \quad \text{and} \quad RMSE_s = \sqrt{\frac{2}{n} \sum_{i=t'+n/2}^{t'+n} (\theta_i - \eta_i)^2} \quad \text{for the first and second halves,}$$

respectively. These RMSEs were computed for all such intervals throughout the simulation, and their respective averages,  $\overline{RMSE_f}$  and  $\overline{RMSE_s}$ , served as indices for adaptability to change and estimation accuracy. Fig. 3 shows the relationship between the adaptability and accuracy for each estimator. Lower values of  $\overline{RMSE_f}$  and  $\overline{RMSE_s}$  indicate superior performance. The figure shows that  $\beta$  varies from 0.05 to 0.25 in increments of 0.005 for both Bayesian and BIB inference. Both methods exhibit a trade-off whereby accuracy corresponds to reduced adaptability. However, the trade-off curve for BIB inference is positioned to the lower left of that for Bayesian inference. The results indicate that BIB inference mitigates the trade-off observed in conventional Bayesian inference.

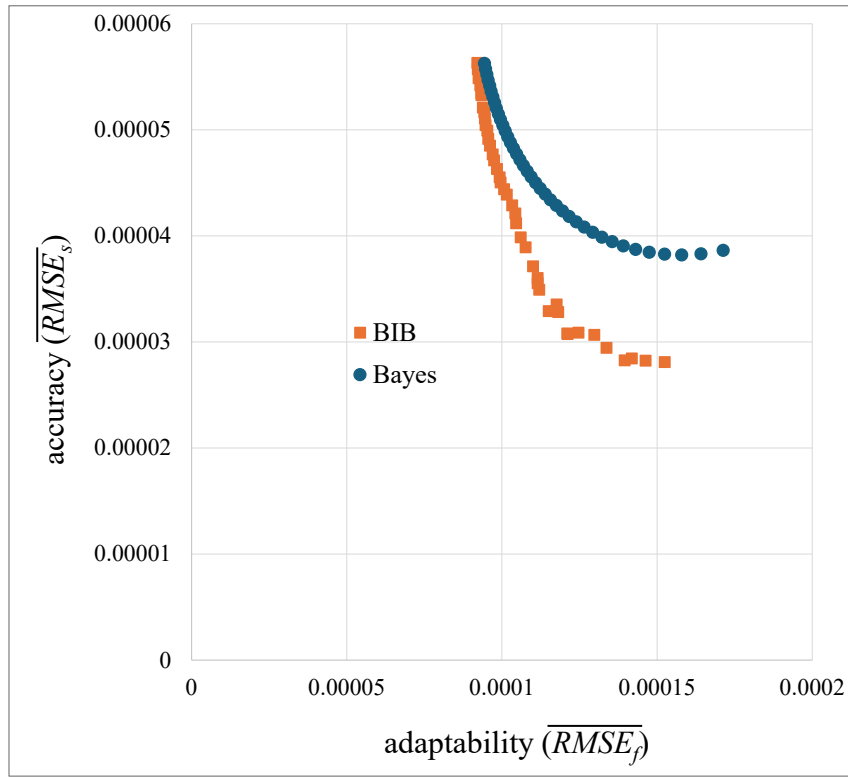
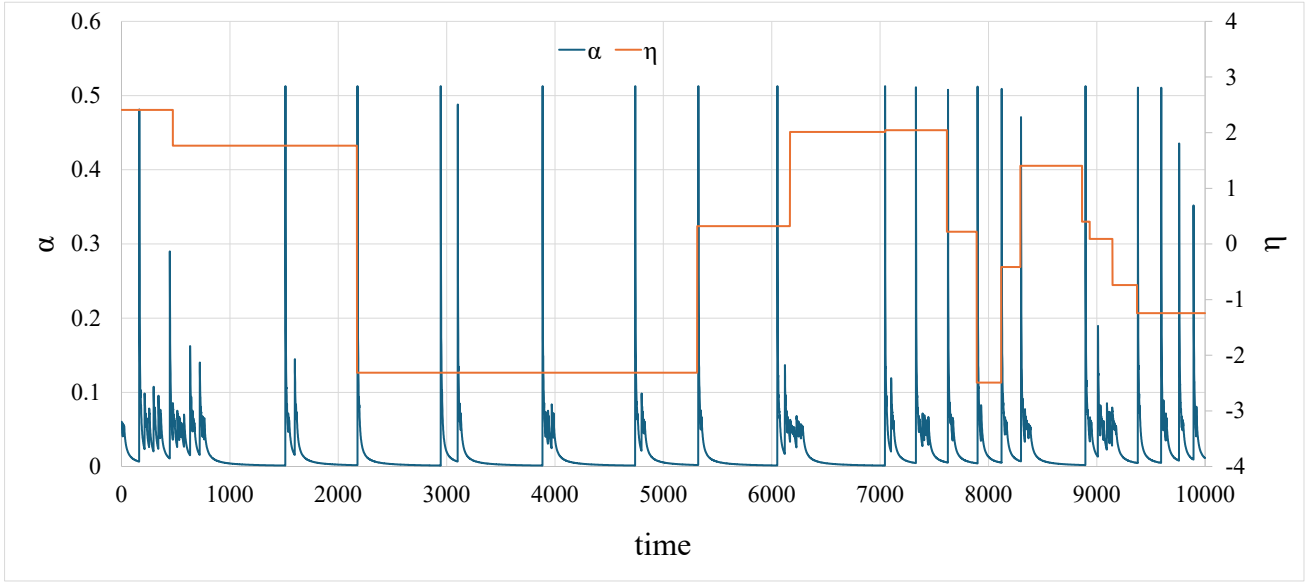
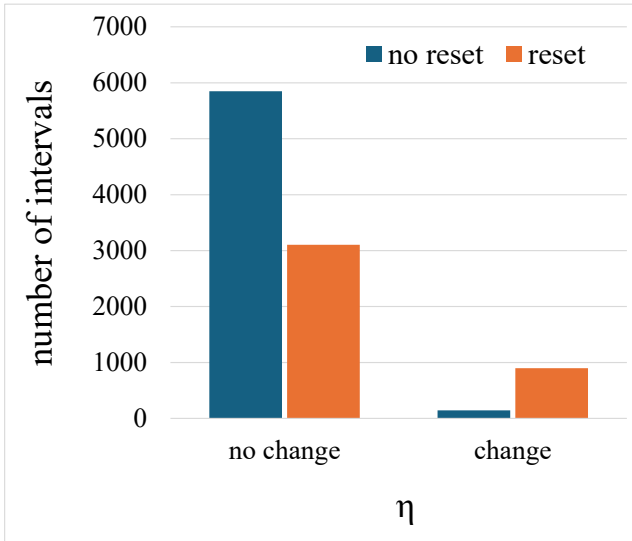


**Fig. 3** Trade-off between adaptability to change and estimation accuracy. The horizontal and vertical axes represent adaptability and accuracy, respectively. Lower values on both axes indicate better the performance

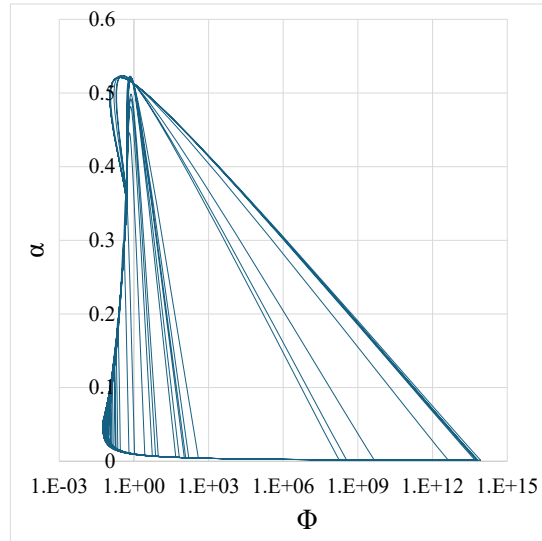




(a)



(b)



(c)

**Fig. 4** Bursts and relaxations in the learning rate during the BIB inference process ( $\beta = 0.05$ ). (a)

Time evolution of the learning rate. The mean value  $\eta$  of the data generating distribution is also

shown. (b) Association between changes in  $\mu$  and bursts in the learning rate. (c) Relationship

between the learning rate and the variance of the prior distribution. The trajectory connects

temporally adjacent data points with lines. The horizontal axis is displayed on a logarithmic scale

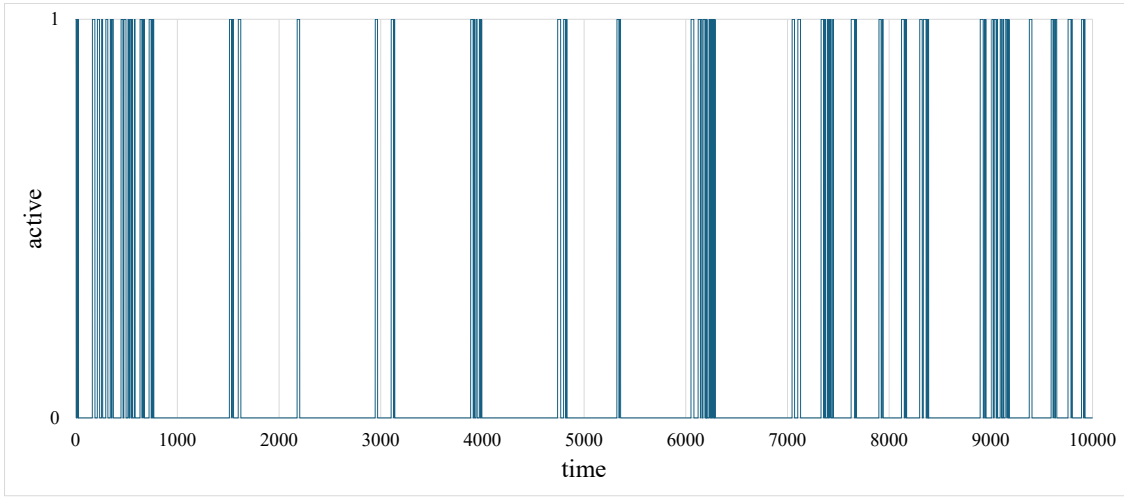
Fig. 4 illustrates the bursts and relaxations in the learning rate observed during the BIB inference process for  $\beta = 0.05$ . Fig. 4(a) presents a representative time series of the learning rate, along with the corresponding time series of the mean  $\eta_t$  of the data-generating distribution. Bursts and relaxations in learning rate occurred intermittently and throughout the time series. Notably, bursts in the learning rate frequently coincided with abrupt changes in  $\eta_t$ . The learning rate  $\alpha$  represents the proportion of external information incorporated into the internal estimate. Hence, it can be interpreted as an indicator of arousal level or sensitivity. Accordingly, the BIB inference mechanism appears to enhance sensitivity in response to significant environmental changes.

The following analyses were conducted to examine this relationship. The simulation period (10,000 steps) was divided into 100 intervals. Subsequently, the following conditions were assessed for each interval:

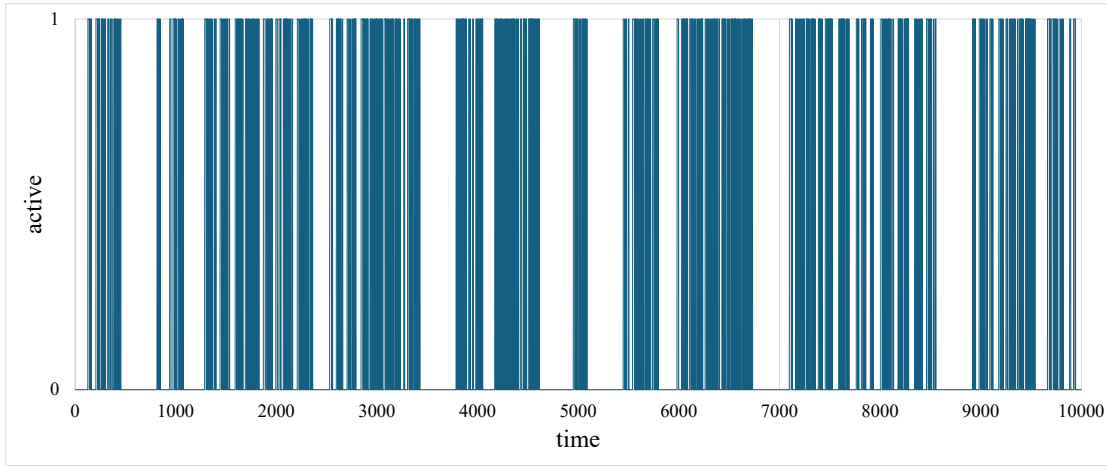
- (i) whether a change in the mean  $\eta$  of the data-generating distribution occurred, and
- (ii) whether bursts occurred in the learning rate.

The number of intervals corresponding to each condition was counted. This simulation was run 100 times with different random seeds. Fig. 4(b) summarizes the results. A chi-square test of independence revealed a significant association between the change in  $\eta$  and the occurrence of learning rate bursts ( $\chi^2(1, N = 2000) = 196.84$ ,  $p = 1.02E - 44$ ,  $V = 0.31$ ). Fig. 4(c) depicts the relationship between the learning rate  $\alpha$  and the variance  $\Phi$  of the prior distribution in BIB inference. Although both quantities vary over time, the figure presents their trajectories in phase space. As noted in the previous section, both  $\alpha$  and  $\Phi$  decrease monotonically and eventually converge to their respective asymptotic values,  $\beta$  and  $\beta\Sigma_0$ , in conventional Bayesian inference. When the discount rate  $\beta$  is large, the learning rate  $\alpha$  also increases, resulting in higher sensitivity to incoming data and faster adaptation to abrupt changes. However, the inherent stochasticity of the observed data leads to reduced estimation accuracy. This trade-off between adaptability and accuracy represents a fundamental limitation of Bayesian inference.

In BIB inference, both the learning rate  $\alpha$  and the prior variance  $\Phi$  initially decreased over time, resembling the behavior observed in standard Bayesian inference. However, unlike in the Bayesian case, the learning rate did not converge to  $\beta$ , but continued to decline. This continued decrease suppressed fluctuations in the estimate, thereby improving accuracy. Notably, once the learning rate  $\alpha$  fell below the discount rate  $\beta$ , the prior variance  $\Phi$  began to increase and eventually diverged. Abrupt increases were observed during the decline trend of  $\alpha$ , corresponding to resets in the inference process; these events appear as bursts in the learning rate. Consequently, the learning rate did not converge to a fixed value in BIB inference but followed a recurring pattern of bursts and relaxations due to the dynamic interaction between likelihood expansion and resetting.



(a)



(b)

**Fig. 5** Example of the time evolution of active and rest states in BIB inference. Active and rest states are represented as 1 and 0, respectively. (a)  $\beta = 0.05$ . (b)  $\beta = 0.1$

The time points at which the learning rate  $\alpha$  exceeds the threshold  $\beta$  are defined as active states, while all other points are classified as rest states. Figs. 5(a) and 5(b) provide time-series examples of active and rest states for the cases of  $\beta = 0.05$  and  $\beta = 0.1$ , respectively. In these figures, active states are indicated by 1, and the rest states by 0. The rest period  $\tau$  is defined as a continuous interval during which the system remains in the rest state. Figs. 6(a) and 6(b) present the complementary cumulative distribution functions (CCDF) of the rest period corresponding to Figs. 5(a) and (b), respectively.

When  $P(\tau)$  follows a power-law distribution ( $P(\tau) \propto \tau^{-\gamma}$ ), the truncated power-law distribution (TP) within the range of  $[\tau_{\min}, \tau_{\max}]$  is expressed as follows for discrete data.

$$P(\tau) = \frac{\tau^{-\gamma}}{\zeta(\gamma, \tau_{\min}, \tau_{\max})}, \quad \zeta(\gamma, \tau_{\min}, \tau_{\max}) = \sum_{i=\tau_{\min}}^{\tau_{\max}} i^{-\gamma} \quad (17)$$

$$CCDF(\tau) = \frac{\zeta(\gamma, \tau, \tau_{\max})}{\zeta(\gamma, \tau_{\min}, \tau_{\max})} \quad (18)$$

However, when  $P(\tau)$  follows an exponential distribution ( $P(\tau) \propto e^{-\lambda\tau}$ ), the EP model is expressed as follows:

$$P(\tau) = (1 - e^{-\lambda}) e^{-\lambda(\tau - \tau_{\min})} \quad (19)$$

$$CCDF(\tau) = e^{-\lambda(\tau - \tau_{\min})} \quad (20)$$

Substituting  $\tau_{\min}$  for  $\tau$  in Eqs. (18) and (20) yields  $CCDF(\tau_{\min}) = 1$ .

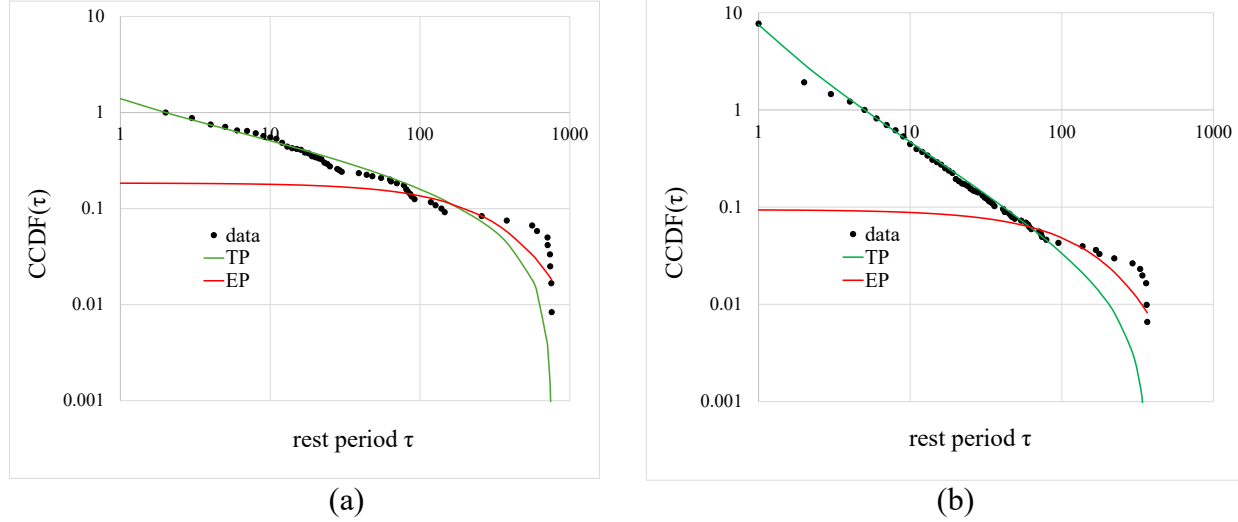
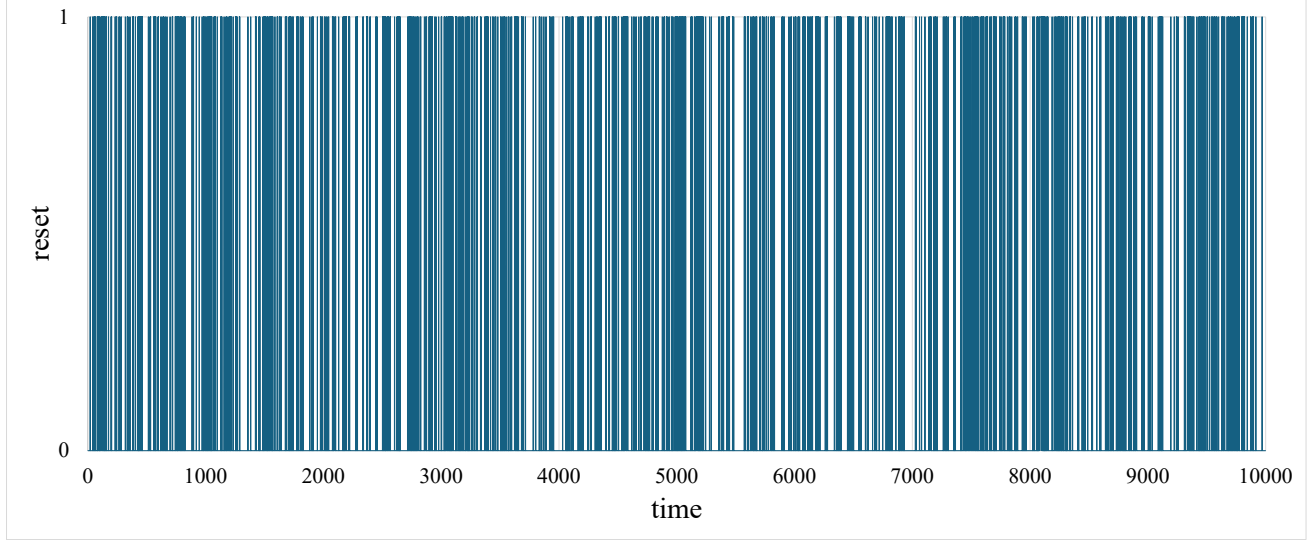


**Fig. 6** CCDF of rest periods corresponding to Figs. 5(a) and 5(b). The fitted results for the TP model (green) and EP model (red) are also shown. (a) CCDF for the case of  $\beta = 0.05$ . Exponent of the TP:  $\gamma = 1.29$ . Fitting range:  $[2, 757]$ . (b) CCDF for the case of  $\beta = 0.1$ . Exponent of the TP:  $\gamma = 2.0$ . Fitting range:  $[5, 366]$

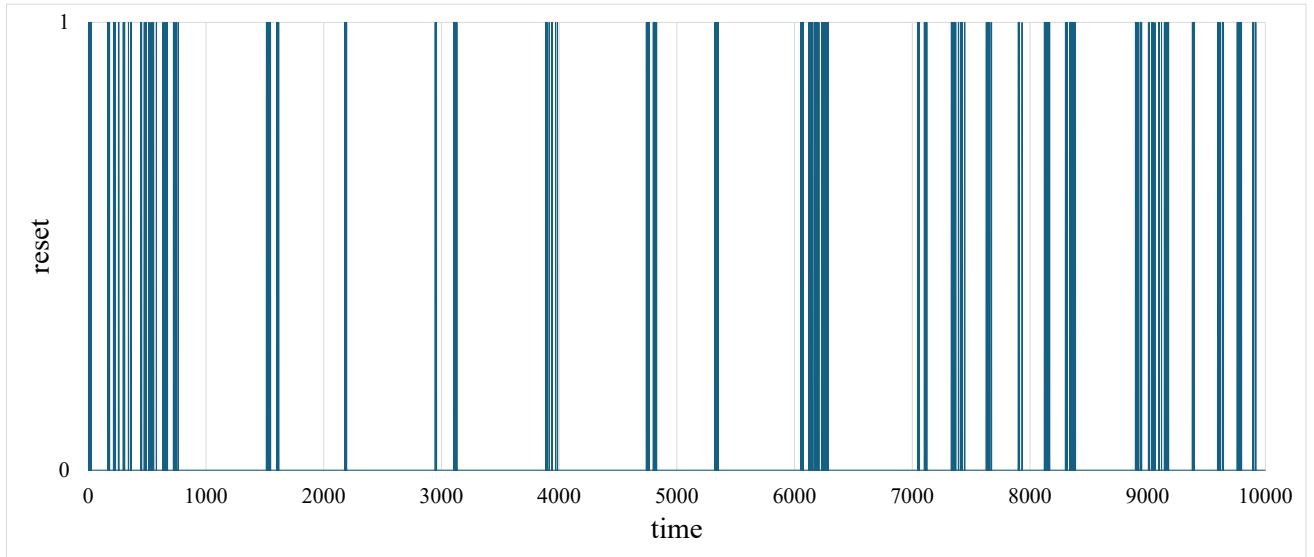
Figs. 6(a) and 6(b) present the results of fitting the TP (green) and EP (red) models to the simulation data. Only the data within the range of  $[\tau_{\min}, \tau_{\max}]$  from the remaining rest period data were used to optimize the fit. The CCDF value in the CCDF plots was set to one at  $\tau = \tau_{\min}$ . Both axes in Figs. 6(a) and 6(b) are displayed on logarithmic scales, forming double logarithmic plots. This representation applies to all subsequent CCDF graphs: The fitting procedures for the frequency distribution of the rest period  $\tau$  to the TP and EP models follow established methods [20–24]. Model parameters were estimated using the maximum likelihood estimation method. Model comparison relied on Akaike information criteria weights, which consider both likelihood and model complexity. Details on parameter estimation, fitting range  $[\tau_{\min}, \tau_{\max}]$ , and model selection criteria are provided in the Supplementary Information.

As shown in Figs. 6(a) and 6(b), the CCDFs of the rest periods (depicted in Figs. 5(a) and 5(b)) are more accurately fitted by the TP model than by the EP model. Across 100 simulations using different random

seeds, the TP model consistently provided a superior fit. The scaling exponent  $\gamma$  exhibited mean values and standard deviations of  $M=1.24$ ,  $SD=0.22$  and  $M=1.57$ ,  $SD=0.28$ , respectively, for  $\beta = 0.05$  and  $\beta = 0.1$ . A t-test showed a statistically significant difference between the two scaling exponents ( $t(198) = -4.72$ ,  $p = 4.49 \times 10^{-6}$ ).



(a)



(b)

**Fig. 7** Example of a time series indicating reset timing for  $\beta = 0.05$ . A value of 1 denotes the occurrence of a reset; 0 denotes no reset. (a) Bayesian inference. (b) BIB inference

Resets of the learning rate or the variance  $\Sigma$  of the likelihood occur in both Bayesian and BIB inferences. However, resets do not produce bursts of learning rate due to the constant value of  $\Sigma$  in Bayesian inference. Fig. 7 illustrates the reset timings in Bayesian and BIB inferences during  $\beta = 0.05$ . Reset times are encoded as 1, and non-reset times as 0. The interval between consecutive resets, referred to as the reset interval, is denoted by  $\Delta t$ .



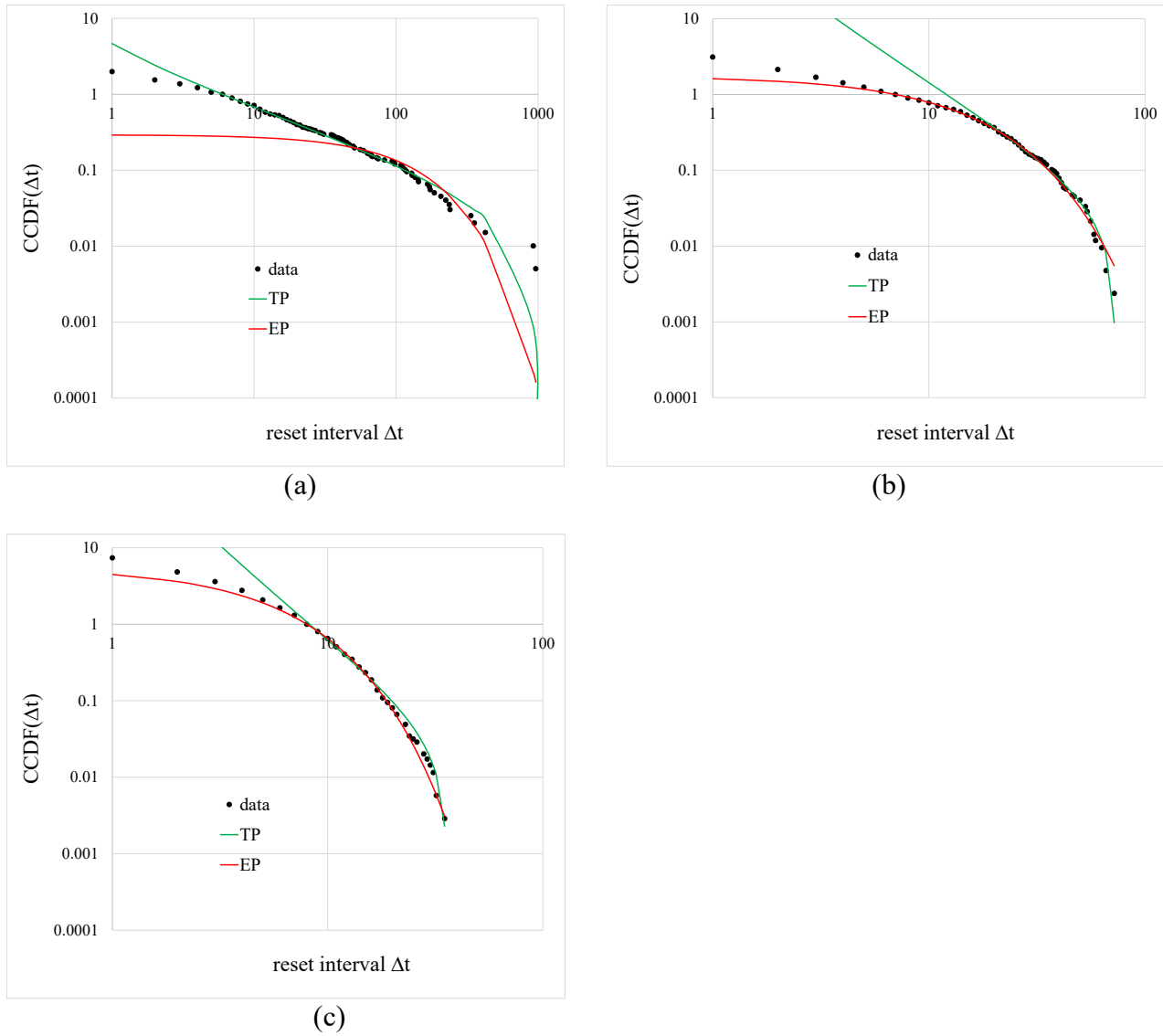


**Fig. 8** CCDF of the occurrence frequency of reset interval in Bayesian inference. Fitted results for the TP model (green) and EP model (red) are also presented. (a) CCDF for the case of  $\beta = 0.01$ .

Exponent of the TP:  $\gamma = 1.68$ . Fitting range:  $[6, 964]$ . (b) CCDF for the case of  $\beta = 0.05$ . Exponent

of the EP:  $\lambda = 0.084$ . Fitting range:  $[7, 72]$ . (c) CCDF for the case of  $\beta = 0.1$ . Exponent of the TP:

$\lambda = 0.21$ . Fitting range:  $[8, 35]$

Fig. 8 presents the CCDF of the occurrence frequency of  $\Delta t$  in the Bayesian inference. Figs. 8(a)–8(c) show the results for  $\beta = 0.01$ ,  $\beta = 0.05$ , and  $\beta = 0.1$ , respectively. The TP model fits better than the EP model

for  $\beta = 0.01$ . The EP model exhibits superior fitting performance for  $\beta = 0.05$  and  $\beta = 0.1$ . Fig. 9 shows the CCDF of the occurrence frequency of  $\Delta t$  in the BIB inference.

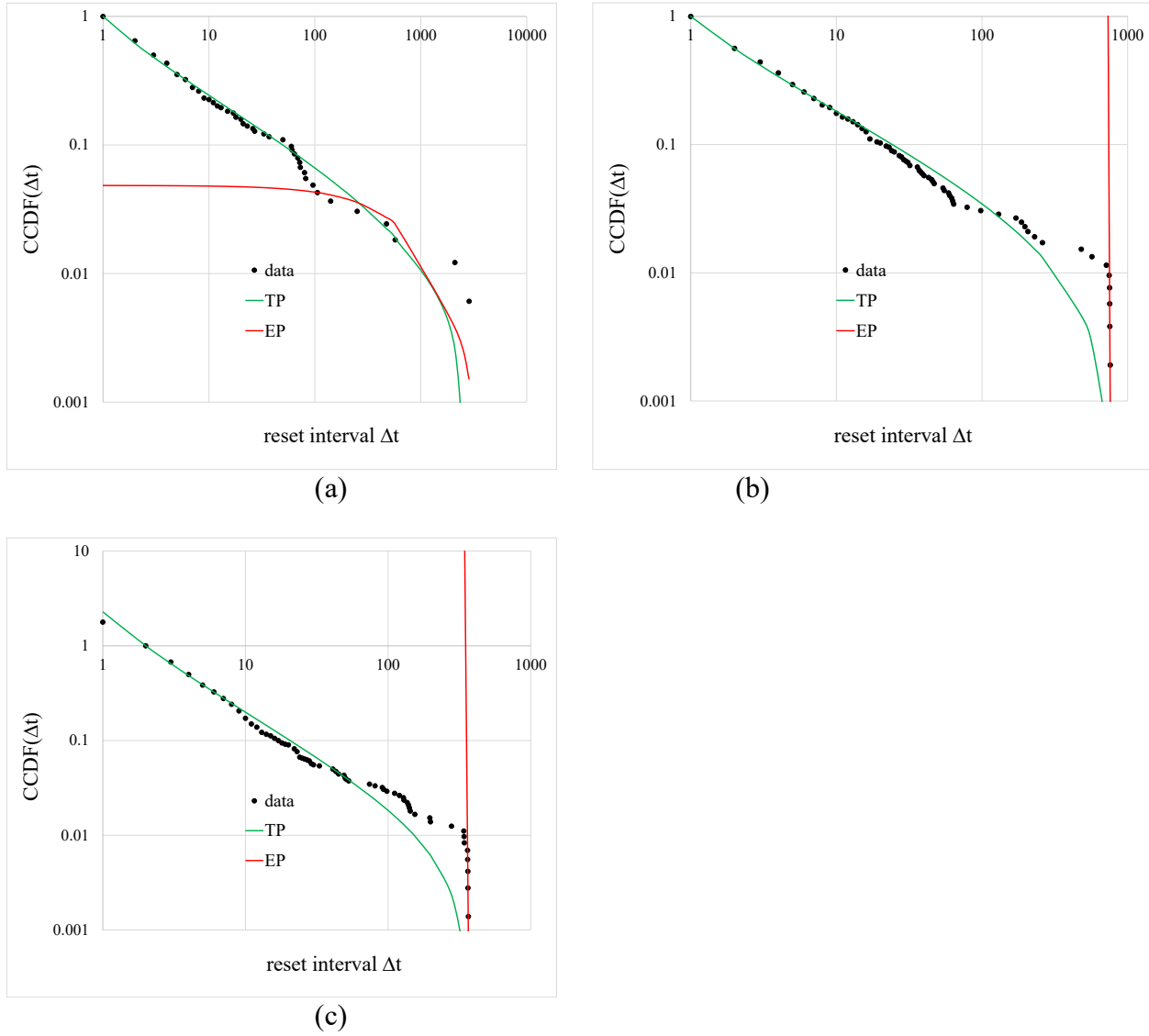


**Fig. 9** CCDF of the occurrence frequency of reset intervals in BIB inference. Fitted results for the TP model (green) and EP model (red) are also presented. (a) CCDF for the case of  $\beta = 0.01$ . Exponent of the TP:  $\gamma = 1.49$ . Fitting range:  $[1, 2861]$ . (b) CCDF for the case of  $\beta = 0.05$ . Exponent of the TP:  $\gamma = 1.59$ . Fitting range:  $[1, 760]$ . (c) CCDF for the case of  $\beta = 0.1$ . Exponent of the TP:  $\gamma = 1.87$ . Fitting range:  $[2, 365]$

Figs. 9(a)–9(c) display the results for  $\beta = 0.01$ ,  $\beta = 0.05$ , and  $\beta = 0.1$ , respectively. The TP model fits better than the EP model in all cases.

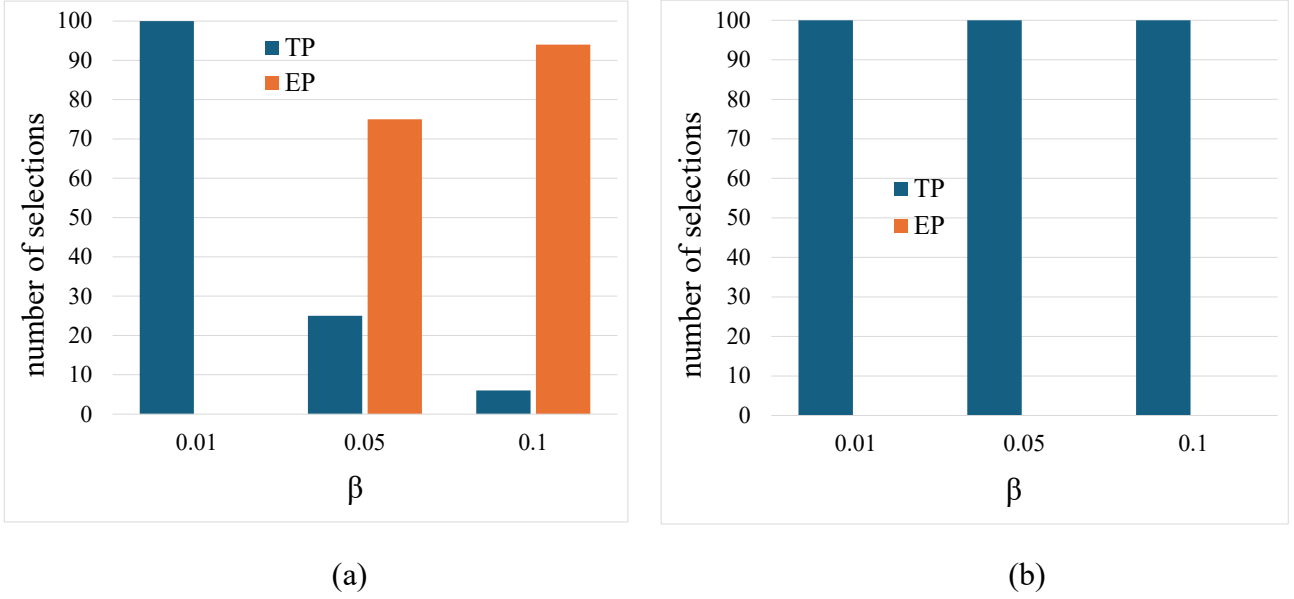


**Fig. 10** Number of selection for each model across 100 simulation runs using different random seeds under the same conditions as those in Figs. 8 and 9. (a) Bayesian inference. (b) BIB inference

We conducted 100 simulations using different random seeds under the same conditions depicted in Figs. 8 and 9. In BIB inference, the TP model was selected in all 100 trials for every value of  $\beta$ . In Bayesian inference, the TP model was selected in all trials for small  $\beta$ , whereas an increasing number of trials favored the EP model as  $\beta$  increased. Figs. 10(a) and 10(b) summarize the results of the Bayesian and BIB inferences, with the horizontal axis representing the value of  $\beta$  and the vertical axis indicating the number of runs selecting each model. A chi-square test revealed a significant association between  $\beta$  and the frequency of model selection in Bayesian inference ( $\chi^2(2, N = 300) = 200.85$ ,  $p = 2.43E - 44$ ,  $V = 0.82$ ).

In Bayesian inference, large values of  $\beta$  lead to a higher learning rate, increasing the impact of observational noise on the estimate  $\theta_t$ , which in turn causes frequent and substantial fluctuations in the prior distribution, resulting in more frequent resets. Conversely, when  $\beta$  is small, the learning rate converges to

zero, stabilizing the estimate  $\theta_t$  and eliminating reset events. Fig. 10(a) shows that the reset interval distribution follows an exponential form for large  $\beta$ , whereas a power-law distribution appears only within a narrow range of  $\beta$  near zero. These findings suggest that power-law behavior in Bayesian inference emerges only in a limited transitional regime between unstable and stable estimation dynamics. In contrast, the BIB inference consistently exhibits power-law reset interval distributions over a broad range of parameter values, indicating that robust scaling behavior arises from the model's intrinsic dynamics.

#### 4 Discussion and conclusions

This study introduced a novel inference model, the BIB inference, by incorporating symmetry bias into Bayesian inference, thereby enabling the concurrent execution of Bayesian and inverse Bayesian updates. However, the BIB inference is not a fundamentally distinct form of inference from the conventional Bayesian inference. Rather, when the strength of the symmetry bias is zero (i.e., when  $\beta = 0$ ), the BIB framework reduces to the standard Bayesian inference. Hence, the conventional Bayesian inference can be considered to be a special case of the more general BIB inference framework.

We applied the proposed model to a task involving the estimation of the mean of a Gaussian distribution generating observed data, where the true mean changed stochastically over time.

First, we confirmed that high learning rates improve adaptability to environmental changes in standard Bayesian inference; however, they reduce estimation accuracy during stable periods due to excessive sensitivity to incoming data. The outcome reflects an inherent trade-off between adaptability and accuracy. However, the BIB inference mitigates this trade-off, achieving both rapid responsiveness to abrupt changes and high accuracy during stable intervals.

This improvement results from the distinct dynamic properties of the learning rate in Bayesian and BIB inferences. In standard Bayesian inference, the accumulation of observational data increases confidence in the estimate, causing the learning rate to gradually decline and eventually converge to a constant value.

However, inverse Bayesian updates enable anomaly detection and hypothesis space resetting in BIB inference, resulting in intermittent bursts and relaxations in the learning rate over time.

Interpreting the learning rate as an index of sensitivity to external stimuli reveals a compelling parallel with biological survival strategies. In stable environments, conserving energy through rest is advantageous, whereas alertness is necessary for responding to unexpected changes. The learning rate in standard Bayesian inference is fixed; hence, high sensitivity incurs a cost to rest, and prioritizing rest reduces environmental responsiveness, rendering the trade-off unavoidable. Certain animals, such as birds and aquatic mammals, have evolved unihemispheric slow-wave sleep (USWS), which enables one hemisphere of the brain to sleep while the other remains awake, thereby balancing energy conservation with vigilance [25]. In BIB inference, a dynamic alteration between active and resting phases emerges naturally during belief updating. When unexpected changes occur, the learning rate spontaneously increases, triggering a transition to a high-sensitivity state. These findings suggest that BIB inference implements a flexible mechanism capable of balancing two critical requirements for biological agents: energy conservation and rapid adaptation to environmental variability.

We analyzed the distribution of rest periods in BIB inference. They consistently exhibited power-law distributions. Although the scaling exponent changed with the discount rate, the scaling structure remained robust, indicating the universality of this dynamic pattern in the proposed model.

Time intervals between behavioral events follow power-law distributions from a biological perspective. For example, the intervals between actions such as sending emails, accessing websites, and posting on social media typically exhibit heavy-tailed power-law characteristics rather than simple exponential patterns [26]. This phenomenon has been attributed to priority-based queuing models, which assume that task execution is governed by priority selection rather than random choice, producing scale-free interevent intervals. However, the universality of this explanation remains under debate [27]. Pfister

and Ghosh [28] extended the priority-based queuing model to consider the statistical properties of time intervals and bursty behavior observed in human smartphone usage, such as screen-touch patterns.

Additionally, notable studies have reported associations between mental disorders and scale-free behavioral dynamics. For instance, in experiments comparing individuals with major depressive disorder and healthy controls, both groups displayed power-law distributions in resting period durations. However, the scaling exponent differed based on the presence of the disorder [29]. Studies on *Drosophila melanogaster* have shown that dopaminergic activity modulates the duration of rest periods, yet the distribution consistently retains a power-law structure [30]. Similarly, while insulin signaling and nutritional conditions influence the temporal characteristics of activity, both active and resting periods follow frequency distributions resembling power laws in *Caenorhabditis elegans* [31]. These findings suggest that even organisms with simple nervous systems can exhibit spontaneous scale-free behavioral patterns that are modulated by internal metabolic states and external environmental conditions.

Next, we analyzed the distribution of reset intervals, defined as the time between changes in the hypothesis with the highest confidence. These reset intervals generally followed an exponential distribution across a broad range of discount rates in standard Bayesian inference. However, a power-law distribution emerged only within a narrow parameter range near the boundary separating stable and unstable regimes. In contrast, the reset intervals—corresponding to the intervals between bursts in the learning rate—consistently exhibited power-law distributions over a broad range of discount rate conditions in BIB inference.

The emergence of scale-free structures is frequently interpreted through the framework of self-organized criticality (SOC). SOC describes a phenomenon wherein a system spontaneously evolves toward a critical state—at the boundary between order and disorder—without requiring detailed fine-tuned external control, thereby exhibiting scale-free behavior [32].

The simulation results presented in this study suggest that the power-law distributions observed under the standard Bayesian inference can be interpreted as manifestations of critical phenomena emerging near the transition between stable and unstable regimes. In such cases, the emergence and reproducibility of critical behavior seem to rely on precise parameter tuning.

In contrast, the proposed BIB inference framework consistently generates power-law distributions across a wide range of parameter settings, without requiring fine-tuning. These findings indicate the presence of a novel scaling mechanism that operates independently of external parameter adjustments, thereby positioning inverse Bayesian updating as a promising candidate for SOC.

The inverse Bayesian updating process emerges naturally through the integration of symmetry bias into conventional Bayesian inference. However, the specific real-world physical phenomenon that this process corresponds to remains unclear. Moreover, experimental evidence is needed to establish whether inverse Bayesian updating, in addition to standard Bayesian updating, is genuinely involved in the reasoning processes of humans and other biological systems. Clarifying this question represents a critical direction for future research.

## References

- [1] Friston, K.J., Kilner, J., Harrison, L.: A free energy principle for the brain. *J. Physiol. Paris* 100, 70–87 (2006). doi: 10.1016/j.jphysparis.2006.10.001
- [2] Friston, K.J., Kiebel, S.: Cortical circuits for perceptual inference. *Neural Netw.* 22, 1093–1104 (2009). doi: 10.1016/j.neunet.2009.07.023
- [3] Hohwy, J.: *The Predictive Mind*. Oxford University Press. <https://doi.org/10.1093/acprof:oso/9780199682737.001.0001> (2013)
- [4] Friston, K.J.: The free-energy principle: a unified brain theory? *Nat. Rev. Neurosci.* 11, 127–138 (2010). doi: 10.1038/nrn2787
- [5] Dehaene, S.: *Consciousness and the Brain: Deciphering How the Brain Codes Our Thoughts*. Viking Press, New York (2014)
- [6] Chater, N., Oaksford, M. (Eds.): *The Probabilistic Mind: Prospects for Bayesian Cognitive Science*. Oxford University Press, England. (2008)
- [7] Sidman, M., Tailby, W.: Conditional discrimination vs. matching-to-sample: an expansion of the testing paradigm. *J. Exp. Anal. Behav.* 37, 5–22 (1982)
- [8] Shinohara, S., Taguchi, R., Katsurada, K., & Nitta, T.: A model of belief formation based on causality and application to N-armed bandit problem. *Transactions of the Japanese Society for Artificial Intelligence*, 22(1), 58–68 (2007). <https://doi.org/10.1527/tjsai.22.58>
- [9] Shinohara, S., Manome, N., Suzuki, K., Chung, U.I., Takahashi, T., Gunji, P.Y., Nakajima, Y. and Mitsuyoshi, S.: Extended Bayesian inference incorporating symmetry bias. *Biosystems*, 190, 104104 (2020).
- [10] Markman, E.M., Wachtel, G.F.: Children’s use of mutual exclusivity to constrain the meanings of words. *Cogn. Psychol.* 20, 121–157 (1988)
- [11] Evans, J.S.B.T., Handley, S.J., Over, D.E.: Conditionals and conditional probability. *J. Exp. Psychol. Learn. Mem. Cogn.* 29, 321–335 (2003)



- [12] Hattori, M., Oaksford, M.: Adaptive non-interventional heuristics for covariation detection in causal induction: model comparison and rational analysis. *Cogn. Sci.* 31, 765–814 (2007)
- [13] Shinohara, S., Manome, N., Suzuki, K., Chung, U.I., Takahashi, T., Okamoto, H., Gunji, Y.P., Nakajima, Y. and Mitsuyoshi, S.: A new method of Bayesian causal inference in non-stationary environments. *PLOS One* 15, e0233559 (2020). <https://doi.org/10.1371/journal.pone.0233559>
- [14] Gunji, Y.-P., Shinohara, S., Haruna, T., Basios, V.: Inverse Bayesian inference as a key of consciousness featuring a macroscopic quantum logical structure. *Biosystems* 152, 44–65 (2017).
- [15] Gunji, Y.-P., Murakami, H., Tomaru, T., Basios, V.: Inverse Bayesian inference in swarming behaviour of soldier crabs. *Philos. Trans. A Math. Phys. Eng. Sci.* 376, 20170370 (2018). <http://dx.doi.org/10.1098/rsta.2017.0370>
- [16] Horry, Y., Yoshinari, A., Nakamoto, Y., Gunji, Y.-P.: Modeling of decision-making process for moving straight using inverse Bayesian inference. *Biosystems* 163, 70–81 (2018).
- [17] Gunji, Y.P., Kawai, T., Murakami, H., Tomaru, T., Minoura, M., Shinohara, S.: Lévy walk in swarm models based on Bayesian and inverse Bayesian inference. *Comput. Struct. Biotechnol. J.* 19, 247–260 (2021). doi: 10.1016/j.csbj.2020.11.045,
- [18] <http://www.mingw.org/> (2025). Accessed 2 May 2025
- [19] <https://www.qt.io/> (2025). Accessed 2 May 2025
- [20] Jansen, V.A.A., Mashanova, A., Petrovskii, S.: Comment on “Lévy walks evolve through interaction between movement and environmental complexity”. *Science* 335, 918 (2012). 10.1126/science.1215747
- [21] Humphries, N.E., Weimerskirch, H., Queiroz, N., Southall, E.J., Sims, D.W.: Foraging success of biological Lévy flights recorded in situ. *Proc. Natl Acad. Sci. U. S. A.* 109, 7169–7174 (2012). <https://doi.org/10.1073/pnas.1121201109>
- [22] White, E.P., Enquist, B.J., Green, J.L.: on estimating the exponent of power-law frequency distributions *Ecology*, 89 (4), 905–912 (2008). 10.1890/07-1288.1 Erratum in: *Ecology* 89, 905–912 (2008). <https://doi.org/10.1890/07-1288.1>

- [23] Clauset, A., Shalizi, C.R., Newman, M.E.J.: Newman Power-law distributions in empirical data in *Siam. Rev* 51, 661–703 (2009). <https://doi.org/10.1137/070710111>
- [24] Edwards, A.M., Phillips, R.A., Watkins, N.W., Freeman, M.P., Murphy, E.J., Afanasyev, V., Buldyrev, S.V., da Luz, M.G., Raposo, E.P., Stanley, H.E., Viswanathan, G.M.: Revisiting Lévy flight search patterns of wandering albatrosses, bumblebees and deer. *Nature* 449, 1044–1048 (2007). <https://doi.org/10.1038/nature06199>
- [25] Rattenborg, N.C., Voirin, B., Cruz, S.M., Tisdale, R., Dell’Omo, G., Lipp, H.P., Wikelski, M., Vyssotski, A.L.: Evidence that birds sleep in mid-flight. *Nat. Commun.* 7, 12468 (2016). <https://doi.org/10.1038/ncomms12468>
- [26] Barabási, A.L.: The origin of bursts and heavy tails in human dynamics. *Nature* 435, 207–211 (2005). doi: 10.1038/nature03459
- [27] Malmgren, R.D., Stouffer, D.B., Motter, A.E., Amaral, L.A.: A Poissonian explanation for heavy tails in e-mail communication. *Proc. Natl Acad. Sci. U. S. A.* 105, 18153–18158 (2008). doi: (21) 10.1073/pnas.0800332105
- [28] Pfister, J.P., Ghosh, A.: Generalized priority-based model for smartphone screen touches. *Phys. Rev. E* 102(1-1), 012307 (2020). doi: 10.1103/PhysRevE.102.012307
- [29] Nakamura, T., Kiyono, K., Yoshiuchi, K., Nakahara, R., Struzik, Z.R., Yamamoto, Y.: Universal scaling law in human behavioral organization. *Phys. Rev. Lett.* 99, 138103 (2007). doi: 10.1103/PhysRevLett.99.138103
- [30] Ueno, T., Masuda, N., Kume, S., Kume, K.: Dopamine modulates the rest period length without perturbation of its power law distribution in *Drosophila melanogaster*. *PLOS One* 7, e32007 (2012). doi: 10.1371/journal.pone.0032007.
- [31] Arata, Y., Shiga, I., Ikeda, Y., Jurica, P., Kimura, H., Kiyono, K., Sako, Y.: Insulin signaling shapes fractal scaling of *C. elegans* behavior. *Sci. Rep.* 12, 10481 (2022). [https://doi.org/10.1038/s41598-022-13022-](https://doi.org/10.1038/s41598-022-13022-6)

[32] Bak, P., Tang, C., Wiesenfeld, K.: Self-organized criticality: an explanation of the  $1/f$  noise. Phys. Rev. Lett. 59, 381–384 (1987). doi: 10.1103/PhysRevLett.59.381

## Funding

This work was supported by JSPS KAKENHI [grant number JP21K12009 and 25K15214].

## Author contributions

**Shuji Shinohara:** Conceptualization, formal analysis, methodology, software, writing, original draft preparation, and funding acquisition. **Daiki Morita:** Software, review, and editing. **Hayato Hirai:** Software, review, and editing. **Ryosuke Kuribayashi:** Software, review, and editing. **Nobuhito Manome:** Writing, reviewing, and editing. **Toru Moriyama:** Writing, reviewing, and editing the manuscript. **Yoshihiro Nakajima:** Writing, reviewing, and editing. **Pegio-Yukio Gunji:** Writing, reviewing, editing, and supervision. **Ung-il Chung:** Writing, review, editing, supervision, and project administration.

## Data availability statement

The code used to perform the simulations in this study is available on GitHub at:

<https://github.com/shinoharaken/BIBinference>.

# **Supplementary Information for**

## **Adaptive Inference through Bayesian and Inverse Bayesian**

### **Inference with Symmetry-Bias in Nonstationary**

### **Environments**

Shuji Shinohara<sup>a,\*</sup>, Daiki Morita<sup>a</sup>, Hayato Hirai<sup>a</sup>, Ryosuke Kuribayashi<sup>a</sup>, Nobuhito Manome<sup>b,c</sup>,  
Toru Moriyama<sup>d</sup>, Yoshihiro Nakajima<sup>e</sup>, Yukio-Pegio Gunji<sup>f</sup>, and Ung-il Chung<sup>b</sup>

<sup>a</sup> School of Science and Engineering, Tokyo Denki University, Saitama, Japan

<sup>b</sup> Department of Bioengineering, Graduate School of Engineering, The University of Tokyo,  
Tokyo, Japan

<sup>c</sup> Department of Research and Development, SoftBank Robotics Group Corp., Tokyo, Japan

<sup>d</sup> Faculty of Textile Science, Shinshu University, Ueda, Japan

<sup>e</sup> Graduate School of Economics, Osaka City University, Osaka, Japan

<sup>f</sup> Department of Intermedia Art and Science, School of Fundamental Science and Technology,  
Waseda University, Tokyo, Japan

\* Corresponding author

E-mail: s.shinohara@mail.dendai.ac.jp

Postal address: School of Science and Engineering, Tokyo Denki University, Ishizaka,  
Hatoyama-machi, Hiki-gun, Saitama 350-0394, Japan

## Fitting to simulation data

### Fitting to truncated power law distribution (TP)

Here, we describe a method to fit the frequency distribution of duration  $\tau$  observed by simulation to the truncated power law distribution (TP). The method was based on references [1-5]. Specifically, we want to find the minimum value  $\hat{\tau}_{\min}$  and maximum value  $\hat{\tau}_{\max}$  of the data to be fitted to the TP and the exponent  $\hat{\gamma}$  of the TP model that best fits the data in the range of  $\hat{\tau}_{\min} \leq \tau \leq \hat{\tau}_{\max}$ . First,  $\hat{\tau}_{\max}$  is the longest step length in the observation data. Next, we describe the method of calculating  $\hat{\tau}_{\min}$ . In the case of a discrete distribution, the TP in the range of  $\tau_{\min} \leq \tau \leq \tau_{\max}$  is expressed by the following formula:

$$P(\tau; \gamma, \tau_{\min}, \tau_{\max}) = \frac{\tau^{-\gamma}}{\zeta(\gamma, \tau_{\min}, \tau_{\max})}, \quad \zeta(\gamma, \tau_{\min}, \tau_{\max}) = \sum_{i=\tau_{\min}}^{\tau_{\max}} i^{-\gamma} \quad (\text{S22})$$

The complementary cumulative distribution functions (CCDF) of  $P(\tau; \gamma, \tau_{\min}, \tau_{\max})$  is expressed in the following equation.

$$CCDF(\tau; \gamma, \tau_{\min}, \tau_{\max}) = \frac{\zeta(\gamma, \tau, \tau_{\max})}{\zeta(\gamma, \tau_{\min}, \tau_{\max})} \quad (\text{S23})$$

If the observed data in the range of  $\tau_{\min} \leq \tau \leq \tau_{\max}$  are  $\{\tau_1, \tau_2, \dots, \tau_n\}$ , then the log-likelihood of these data for TP is calculated using equation (S1) as follows:

$$L(\gamma; \tau_{\min}, \tau_{\max}) = \sum_{i=1}^n \ln P(\tau_i; \tau_{\min}, \tau_{\max}, \gamma) = -n \ln \zeta(\gamma, \tau_{\min}, \tau_{\max}) - \gamma \sum_{i=1}^n \ln \tau_i \quad (\text{S24})$$

The exponent  $\hat{\gamma}(\tau_{\min}, \tau_{\max})$  of the TP model that best fits the data in the range of  $\tau_{\min} \leq \tau \leq \tau_{\max}$  is  $\gamma$ , which maximizes  $L(\gamma; \tau_{\min}, \tau_{\max})$ . Specifically, we varied  $\gamma$  from 0.5 to 3.5 in increments of 0.01 to obtain  $\hat{\gamma}(\tau_{\min}, \tau_{\max})$ , which numerically maximizes equation (S3).

We introduce the Kolmogorov-Smirnov static  $D(\tau_{\min}, \tau_{\max})$  to measure the closeness of the CCDF  $S(\tau; \tau_{\min}, \tau_{\max})$  created from the data in the range of  $\tau_{\min} \leq \tau \leq \tau_{\max}$  and the  $CCDF(\tau; \hat{\gamma}(\tau_{\min}, \tau_{\max}), \tau_{\min}, \tau_{\max})$  represented by equation (S2).

$$D(\tau_{\min}, \tau_{\max}) = \max_{\tau_{\min} \leq \tau \leq \tau_{\max}} \left| S(\tau; \tau_{\min}, \tau_{\max}) - CCDF(\tau; \hat{\gamma}(\tau_{\min}, \tau_{\max}), \tau_{\min}, \tau_{\max}) \right| \quad (\text{S25})$$

If we fix  $\tau_{\max} = \hat{\tau}_{\max}$ , then  $D(\tau_{\min}, \hat{\tau}_{\max})$  is a function of  $\tau_{\min}$ . We numerically choose  $\tau_{\min}$  out of the observed data, which minimizes  $D(\tau_{\min}, \hat{\tau}_{\max})$ . That is,  $\hat{\tau}_{\min} = \arg \min_{\tau_{\min}} D(\tau_{\min}, \hat{\tau}_{\max})$ . In the above,  $\hat{\tau}_{\min}$  and  $\hat{\tau}_{\max}$

were obtained. Finally, we find the exponent  $\hat{\gamma} = \hat{\gamma}(\hat{\tau}_{\min}, \hat{\tau}_{\max})$  of the TP model that best fits the data in the range of  $\hat{\tau}_{\min} \leq \tau \leq \hat{\tau}_{\max}$  using the formula (S3).

### Fitting to exponential distribution (EP)

In this section, our goal is to find the minimum value  $\hat{\tau}_{\min}$  of the observed data to be fitted to the exponential distribution (EP) model and the exponent  $\hat{\lambda}$  of the EP model that best fits the data in the range of  $\hat{\tau}_{\min} \leq \tau$ . In the discrete case, the EP in the range of  $\tau_{\min} \leq \tau$  is expressed in the following equation:

$$P(\tau; \tau_{\min}, \lambda) = (1 - e^{-\lambda}) e^{-\lambda(\tau - \tau_{\min})} \quad (\text{S26})$$

The CCDF of  $P(\tau; \tau_{\min}, \lambda)$  is expressed as follows:

$$CCDF(\tau; \tau_{\min}, \lambda) = e^{-\lambda(\tau - \tau_{\min})} \quad (\text{S27})$$

If the data in the range of  $\tau_{\min} \leq \tau$  is  $\{\tau_1, \tau_2, \dots, \tau_m\}$ , then the log likelihood for these data is expressed as:

$$L(\lambda; \tau_{\min}) = \sum_{i=1}^m \ln P(\tau_i; \tau_{\min}, \lambda) = m \ln(1 - e^{-\lambda}) - \lambda \sum_{i=1}^m (\tau_i - \tau_{\min}) \quad (\text{S28})$$

The exponent  $\hat{\lambda}(\tau_{\min})$  that maximizes  $L(\lambda; \tau_{\min})$  is found as a solution to  $\frac{\partial L(\lambda; \tau_{\min})}{\partial \lambda} = 0$  by the following formula:

$$\hat{\lambda}(\tau_{\min}) = \ln \left( \frac{m}{\sum_{i=1}^m (\tau_i - \tau_{\min})} + 1 \right) \quad (\text{S29})$$

$\hat{\tau}_{\min}$  is calculated from the simulation data and  $D_{adj}$  obtained from equation (S6), as in the case of TP. The final value is

$$\hat{\lambda} = \hat{\lambda}(\hat{\tau}_{\min}).$$

### Comparison of truncated power law distribution (TP) and exponential distribution (EP)

In this section, we describe a method to determine which of the two distribution models, TP or EP, is more suitable for the simulation data. We use Akaike Information Criteria weights (AICw) for comparison [14]. First, the Akaike Information Criterion (AIC) for data in the range of  $\tau_{\min} \leq \tau \leq \tau_{\max}$  is defined as follows:

$$\begin{aligned}
AIC_{TP} &= -2 \ln \left( L \left( \hat{\gamma}; \tau_{\min}, \tau_{\max} \right) \right) + 2 \\
AIC_{EP} &= -2 \ln \left( L \left( \hat{\lambda}; \tau_{\min} \right) \right) + 2
\end{aligned} \tag{S30}$$

The AIC difference  $\Delta$  is then calculated as follows:

$$\begin{aligned}
AIC_{\min} &= \min(AIC_{TP}, AIC_{EP}) \\
\Delta_{TP} &= AIC_{TP} - AIC_{\min} \\
\Delta_{EP} &= AIC_{EP} - AIC_{\min}
\end{aligned} \tag{S31}$$

Finally, AICw are calculated as follows:

$$\begin{aligned}
w_{TP} &= \frac{e^{-\Delta_{TP}/2}}{e^{-\Delta_{TP}/2} + e^{-\Delta_{EP}/2}} \\
w_{EP} &= \frac{e^{-\Delta_{EP}/2}}{e^{-\Delta_{TP}/2} + e^{-\Delta_{EP}/2}}
\end{aligned} \tag{S32}$$

First, using the data in the range of  $\hat{\tau}_{\min} \leq \tau \leq \hat{\tau}_{\max}$  calculated during the fitting of the TP, we find the most appropriate exponents  $\hat{\gamma}$  and  $\hat{\lambda}$  for each model.

Next, these exponents are used to calculate and compare AICw. Then, we change  $\hat{\tau}_{\min}$  to the one calculated during the fitting of the EP and compare. If  $w_{TP} > w_{EP}$  for both data, the TP is considered to fit the simulated data better. On the other hand, if  $w_{TP} < w_{EP}$  for both data, the EP is considered to fit the simulated data better. In case of discrepancies between the results in both data, the following indicators were defined and judged according to reference [10].

$$\begin{aligned}
D_{adj, TP} &= \frac{\ln N}{\ln n_{TP}} D_{TP} \\
D_{adj, EP} &= \frac{\ln N}{\ln n_{EP}} D_{EP}
\end{aligned} \tag{S33}$$

where  $D_{TP}$  and  $D_{EP}$  are the Kolmogorov-Smirnov static calculated during the model fitting of the TP and EP, respectively.  $N$  is the total number of observed data points, and  $n_{TP}$  and  $n_{EP}$  are the number of observed data points used in each model fitting. In other words, the index considers a model that can fit more observational data to be a better model. In the case of  $D_{adj, TP} < D_{adj, EP}$ , the TP is considered to fit the simulation data better. Conversely, when  $D_{adj, TP} > D_{adj, EP}$ , EP is considered to be a better fit to the simulation data.

## REFERENCES

1. N. E. Humphries et al. Foraging success of biological Lévy flights recorded in situ. *Proceedings of the National Academy of Sciences of the United States of America* vol. 109,19 (2012): 7169-74. doi:10.1073/pnas.1121201109
2. V. A. Jansen, A. Mashanova, and S. Petrovskii. Comment on "Lévy walks evolve through interaction between movement and environmental complexity". *Science*. 2012 Feb 24;335(6071):918; author reply 918. doi: 10.1126/science.1215747. PMID: 22362991.
3. E. P. White, B. J. Enquist, J. L. Green. On estimating the exponent of power-law frequency distributions. *Ecology*. 2008 Apr;89(4):905-12. doi: 10.1890/07-1288.1. Erratum in: *Ecology*. 2008 Oct;89(10):2971. PMID: 18481513.
4. A. Clauset, C. R. Shalizi, and M. E. J. Newman, Power-Law Distributions in Empirical Data *SIAM Rev.*, 51(4), 661–703
5. A. M. Edwards, R. A. Phillips, N. W. Watkins, M. P. Freeman, E. J. Murphy, V. Afanasyev, S. V. Buldyrev, M. G. da Luz, E. P. Raposo, H. E. Stanley, and G. M. Viswanathan. Revisiting Lévy flight search patterns of wandering albatrosses, bumblebees and deer. *Nature*. 2007 Oct 25;449(7165):1044-8. doi: 10.1038/nature06199. PMID: 17960243.